

Peptide Engineered Microcantilevers for Selective Chemical Force Microscopy and Monitoring of Nanoparticle Capture

M. Munz⁺, A. Bella, S. Ray⁺⁺, N.C. Bell, A.G. Shard, C. Minelli*

Analytical Science Division, National Physical Laboratory, Hampton Road, Teddington
TW11 0LW, UK

Abstract

Engineered peptides capable of binding to silica have been used to provide contrast in chemical force microscopy (CFM) and tested for their capacity to selectively capture silica nanoparticles (NPs). Gold coated atomic force microscopy (AFM) microcantilevers with integrated tips and colloidal probes were functionalised with engineered peptides through a thiol group of a terminal cysteine which was linked via a glycine trimer to a 12-mer binding sequence. The functionalised probes demonstrated a significantly increased binding force on silicon oxide areas of a gold-patterned silicon wafer, whereas plain gold probes, and those functionalised with a random permutation of the silica binding peptide motif or an all-histidine sequence displayed similar adhesion forces to gold and silicon oxide. As the functionalised probes also allowed contact mode imaging subsequently to the adhesion mapping, also the associated friction contrast was measured and found to be similar to the adhesion contrast. Furthermore, the adsorption of silica NPs onto planar gold surfaces functionalised in the same manner was observed to be selective. Notably, the surface

coverage with silica NPs was found to decrease with increasing pH, implying the importance of electrostatic interactions between the peptide and the NPs. Finally, the adsorption of silica NPs was monitored via the decrease in fundamental resonance frequency of an AFM microcantilever functionalised with silica binding peptides.

Keywords: Genetically engineered peptides for inorganics (GEPI); Silica (SiO₂) nanoparticles; Atomic force microscopy (AFM); Chemical force microscopy (CFM); adhesion; adsorption; waste water remediation;

* *Corresponding author:* Dr Caterina Minelli, e-mail: caterina.minelli@npl.co.uk, phone: +44 20 8943 6689

+ *Present address:* Department of Chemistry, The University of Sheffield, Sheffield S3 7HF, UK

++ *Present address:* Environment and Technology, University of Brighton, Brighton BN2 4GJ, UK

I. INTRODUCTION

Proteins and peptides are promising ingredients for the fabrication of bio-inorganic interfaces, as they are known to mediate adhesion and thus enable the growth of biological materials that are often highly organised at the macroscopic and nanoscopic levels. Mineralised tissues, such as bones, teeth, spines or shells, contain proteins which function as binding agents for the mineralisation process.^{1,2} In addition, proteins allow for the modification of biomaterial surfaces to confer recognition and selectivity.³ Considerable efforts have been made to utilise proteins and protein-derived molecules for the controlled assembly of nanostructured materials.^{4, 5, 6, 7, 8}

A time-effective approach to select solid-binding peptides with a high binding affinity to a specific target material is combinatorial display technology, an approach based on iterative affinity selection procedures.⁴ Typically, such biopanning protocols involve phage display or cell-surface display techniques.^{4, 5, 8} Peptides singled out by such a genetic selection process are frequently referred to as genetically engineered peptides. More specifically, they are referred to as genetically engineered peptides for inorganics (GEPs) if they were designed to bind to inorganic materials.^{1, 5, 9}

Using such affinity selection procedures, peptides have been identified that bind selectively to specific inorganic materials⁸, including metals (Au^{10, 11, 12}; Al¹³; Pt¹⁴; Pd¹²; Ti^{15, 16}), oxides and semiconductors (CuO₂ and Cu₂O⁷; GaAs¹³; CdS¹⁷; ZnS^{11, 17}; ZnO^{18, 19}) and minerals (hydroxyapatite²⁰; calcite^{5, 21}; sapphire²²). Also selective binding to organic compounds such as carbon nanotubes²³, graphite²⁴, graphene²⁵ and polymers^{3, 26} has been demonstrated.

Sanghvi et al.³ identified a peptide that selectively binds to polypyrrole, an electrically conductive polymer. Jaworski et al.²⁶ developed a gas sensor for explosives, involving a highly selective receptor based on peptides.

To quantify the selective binding behaviour of engineered peptides, a measurement technique for adhesion forces is needed and, ideally, sufficient spatial resolution to identify different areas of a chemically heterogeneous or patterned surface. Atomic force microscopy (AFM) meets these requirements, via force measurements between a surface and a sharp tip attached to a micro-cantilever.^{27, 28} Spatial variations in the force interaction of a surface with a certain molecular species can be measured by covalently attaching such molecules to the AFM tip and recording force-distance curves (FDCs) over an array of spots on the surface (force volume mode). This approach of force measurements as a function of the AFM tip chemistry is frequently referred to as chemical force microscopy (CFM).^{29, 30, 31, 32, 33, 34} Alternatively to the measurement of FDCs, contrasts related to surface chemistry can be obtained in lateral force microscopy (LFM), that is, by imaging in contact mode and recording the torsional cantilever deformation resulting from friction forces between AFM probe and surface.^{30, 33, 34, 35, 36, 37}

Typically, functionalisation strategies for CFM are based upon silane or thiol chemistry to modify silicon or gold coated AFM probes with molecules that bind to constituents of the surface under investigation.^{30, 32, 33, 34} In the case of biomolecules, specific force measurements can be achieved through molecular recognition, e.g. ligand-receptor binding where selective interactions result from several bonds assisted by the shape of the binding molecules.^{31, 34, 38} In the case of simple organic molecules or inorganic surfaces, however, the level of chemical selectivity afforded by common functionalisation strategies is comparatively low. Significant improvement should arise from the availability of engineered peptides selected from combinatorial peptide libraries, and promising work taking this approach has been reported.¹⁶ Using AFM tips modified with a titanium binding peptide, Arai et al.¹⁶ demonstrated CFM of patterned Au/Ti surfaces in water.

Effective exploitation of the peptide binding behaviour needs guiding rules to tailor peptides and achieve the required levels of selectivity and specificity.⁸ In general, the selectivity of a peptide or protein for a surface can originate from both chemical and structural recognition.³⁹ The former may involve short- and long-range forces, including hydrogen bonding, Coulomb forces, dipole-dipole interactions and van der Waals forces.^{40, 41, 42} The latter may involve molecular conformation, folding, size or surface morphology.^{41, 43, 44} Often, genetically engineered peptides do not reveal any specific conformation, and the surface-binding properties may be driven by an adaptation of peptide residues to the interfacial features existing on metal surfaces.⁵

In an extensive study of the binding behaviour of fluorescently tagged homopeptides, Willett et al.¹³ demonstrated that increased adhesion levels occur preferably between insulator surfaces and homopeptides made of the amino acids arginine, lysine, histidine, aspartic acid and glutamic acid (R, K, H, D and E, respectively)⁴⁵ with charged side groups. Several studies have shown that charged residues play an important role^{3, 7, 11, 13, 46, 47}, but other factors may be of comparable relevance, such as the way the peptide is presented to the material and the way the structure deforms upon surface binding.^{7, 8, 48} Notably, histidine (H)⁴⁵ has been employed abundantly in engineered peptides.^{11, 46, 49} It has a polar, basic side chain and is known for binding to nickel⁵⁰, iron and zinc^{49, 51}. Furthermore, homohexamers of H⁴⁵ were found to bind to several II-VI semiconductors¹¹, thus indicating that its binding behaviour is not highly selective. Hence, selectivity may need a variety of residues in a sequence, with both the type and order of residues being of relevance. As a starting point to study the effects of adjacent residues, heteropeptides made of two different residues were investigated. In an analysis of interdigitated peptide sequences of the general form XHXHXHX, with X representing one of the 20 natural amino acids, the residues K and W⁴⁵ were found to increase the level of adhesion.¹¹ These findings would suggest that material

specificity can be improved by adding structural constraints that favour certain bond angle ranges.

Here, we evaluated the potential of the Si4-1 silica-binding peptide motif presented and tested by Naik et al.^{5,52}, for both CFM and selective adsorption of silica NPs. AFM force mapping using probes functionalised with SiO₂ binding peptides demonstrated an increased adhesion force on SiO₂ areas of a patterned test sample, whereas a vanishing adhesion contrast was found in the case of control experiments. Based on the observed selective binding behaviour, we suggest a CFM approach which is augmented in that it allows chemically selective measurements by utilising engineered peptides for functionalisation of AFM probes.

Furthermore, the binding of silica NPs has been studied for a range of pH values, employing scanning electron microscopy (SEM) to evaluate the area density of NPs adsorbed on peptide film surfaces. Finally, we show that peptide-engineered AFM cantilevers can be utilised to monitor surface adsorption of NPs through measurements of the AFM cantilever resonance frequency, which decreases due to an increase in total cantilever mass upon adsorption of NPs. Hence, by example of an established silica binding peptide motif, we demonstrate an improved approach to CFM as well as NP capture that allows a high level of chemical selectivity. The approach can be expected to be applicable to a variety of inorganic surfaces provided availability of peptides with suitable binding characteristics. Yet it is interesting to note that silica NPs are of relevance to a range of application areas, including NP based sensing^{53, 54, 55}, drug delivery⁵⁵, or surface engineering^{56, 57, 58}. Moreover, silica is a common choice for particle size reference materials^{59, 60, 61}.

II. MATERIALS AND METHODS

Peptides: Engineered peptides were purchased from GenScript (Piscataway, NJ) and are described in Table 1. The peptide gSi4-1 contains the silica-binding peptide motif Si4-1 described by Naik et al.^{5, 52}, but also includes a terminal C and an adjacent GGG trimer. The peptide gSi4-1s contains a motif having the same number of the same amino acids found in gSi4-1, but displayed in a random order (scrambled sequence). Importantly, gSi4-1s has the same mass and charge as gSi4-1, but a different amino acid order and, for this reason, was utilised to analyse whether the amino acid order in the silica-peptide interaction is important.

TABLE 1. Peptides used in this study, their molecular weight, MW, in unified atomic mass units (u) and their isoelectric pH value, pI.

Name ^a	Sequence ^b	MW ^c	pI ^c
gSi4-1	CGGGMSPHPHPRHHHT	1786.0	8.1
gSi4-1s	CGGGHTHPHHMHRPSP	1786.0	8.1
gHis12	CGGGHHHHHHHHHHHH	1979.0	7.7
gAG4	CGGGNPSSLFRYLPSD ^d	1711.9	5.6

^a Original names⁵² are used, *g* and *s* denote gold-binding and scrambled respectively; ^b All peptides are capped by acetylation; ^c Values calculated using https://www.genscript.com/ssl-bin/site2/peptide_calculation.cgi; ^d No amidation.

In view of the high number of H residues found in gSi4-1, a further control peptide was utilised, gHis12, where all the amino acids of the peptide sequence were replaced by H⁴⁵. All the peptides were designed to have a unique N-terminal cysteine residue to direct their binding to gold and a tri-glycine spacer to confer flexibility to the orientation and movement of the main peptide sequence. Stock peptide solutions of ~1 mM concentration were prepared

in ultrapure water (resistivity $> 18 \text{ M}\Omega \text{ cm}$). Their concentration was measured by absorption spectroscopy (Lambda 850 UV-Vis spectrometer, Perkin Elmer, MA) through the peptide extinction coefficient.⁶² For calculation of the peptide isoelectric point, pI, a routine was used that sums up the pI values of its amino acids and end groups.⁶³ An additional control peptide was gAG4, which is derived from a sequence first described by Naik et al.⁶⁴ and has a binding affinity for silver.

Test surfaces for CFM: The test surfaces for CFM measurements consisted of thermally oxidised Si chips (Si<100> wafer with a 10 nm thermal oxide layer) which were patterned with a regular array of gold squares. Employing a coater deposition system (tectra, Germany), periodic square areas of gold on thermally oxidised Si chips were produced by thermal evaporation, using a copper square mesh with a pitch size of $\sim 12.7 \mu\text{m}$ (type G2786C, Agar Scientific, UK) as a mask. Before each AFM measurement the test surface was treated in an UV/ozone cleaner for ~ 25 min to remove organic contaminations. After ~ 5 AFM sessions, it was also cleaned in a Piranha solution, a 3:1 mixture of concentrated sulfuric acid (H_2SO_4) to 30% hydrogen peroxide (H_2O_2) solution (**Caution:** *Piranha solution reacts violently with organic matter and should be handled with extreme care*).

CFM probes: Gold coated AFM probes were used to measure the adhesion force between synthetic peptides and test surfaces. Their spring constant was determined via the thermomechanical method which analyses the thermally driven fundamental resonance.^{65, 66} Typically, the uncertainty of this calibration method is below $\sim 10\%$.⁶⁶ Employing the optical viewing system of the Cypher AFM (Asylum Research, Santa Barbara, CA), the laser spot was carefully placed nearby the free end of the AFM cantilever, thus minimising uncertainties associated with variations in the laser spot position. Both AFM probes with an integrated tip and with a colloidal probe were used. The former were of the type BL-RC-150VB (Olympus, Japan) with a typical tip radius of $R \sim 25 \text{ nm}$ and a typical normal spring

constant of $k_z \sim 80$ pN/nm. The latter were of type CP-PNPL-Au-A (Sqube, Germany) with a probe radius in the range $R \sim 1.5 - 3$ μm and a spring constant of $k_z \sim 30$ pN/nm. Both types of probes were gold coated to allow for chemical attachment through thiol chemistry.

Subsequently to treatment in an UV/ozone cleaner (Uvocs, Philadelphia) for ~ 15 min, the AFM probes were functionalised by dipping for ~ 100 s into a 1 mM aqueous solution of the peptides. Immediately after the dip coating, the probes were washed in deionized water to remove excess amounts of the peptides.

CFM measurements: For all force mapping and LFM measurements, a Cypher AFM system was employed. The instrument was operated in a laboratory controlled to (22 ± 1) $^\circ\text{C}$ and (44 ± 10) % relative humidity. It was calibrated with an NPL-traceable blaze grating and a step height standard to $\sim 6\%$ relative uncertainty. To prevent optical interference effects which may cause oscillations of the deflection signal, the laser for readout of the cantilever deflection was replaced with a superluminescent diode (Asylum Research). All CFM measurements were taken in a 10 mM sodium phosphate buffer solution containing ~ 0.2 wt% Tween20 (Poly(oxyethylene) sorbitan monolaureate $\text{C}_{58}\text{H}_{114}\text{O}_{26}$; Sigma Aldrich), a non-ionic surfactant that is frequently used to suppress non-specific interactions^{15, 67}. The buffer pH was in the range 5.5 to 6. Force maps were measured over an area of 20×20 μm^2 with a pixel resolution of 32×32 . Typically, the z -velocity of the probe was ~ 1.4 $\mu\text{m}/\text{s}$ thus resulting in a total scan time of ~ 45 min. Subsequently to the force mapping, the area was imaged in LFM mode to measure spatial variations in the friction force between probe and test sample. For analysis of the AFM data, the software packages Scanning Probe Image Processor SPIP version 6.1.0 (Image Metrology, Denmark) and Gwyddion 2.41 (Czech Metrology Institute, Brno, Czech Republic) were employed, in addition to the Asylum Research software.

Cantilever mass balance: Cantilevers of type BL-AC40TS from Olympus were mounted on a Cypher AFM system and immersed into drops of the plain buffer or a NP suspension with

SiO₂ NPs of ~100 nm diameter. Employing the AFM setup, thermally activated oscillations of the cantilever were monitored in-situ. A spectrum was obtained after Fourier-transformation of the cantilever deflection signal and the peak frequency determined via a fit of the harmonic oscillator model to the fundamental resonance peak. The buffer was a 10 mM sodium phosphate solution at pH 5.5. For functionalisation with SiO₂ binding peptides, the cantilevers were treated in the same manner as the cantilevers used for force mapping measurements (see above). Owing to the gold reflex coating of BL-AC40TS type probes, the cantilever side opposite to the tip side is suitable for functionalisation with the SiO₂ binding peptide gSi4-1 used for the CFM measurements. The cantilevers are made of silicon nitride and of rectangular shape with a length of (38 ± 10) μm and a width of (16 ± 1) μm (data provided by the manufacturer). In air, the cantilever resonance frequency was in the range from ~81 to 92 kHz and the spring constant in the range from ~45 to 81 pN/nm.

Nanoparticles: Stöber silica particles⁶⁸ were synthesized following the protocol of Kim *et al.*⁶⁹ Tetraethyl orthosilicate (TEOS) ($\geq 99\%$), methanol, ammonium hydroxide (~30%) and isopropanol were used as received from Sigma-Aldrich (St. Louis, MO). Briefly, ultrapure water and ammonium hydroxide were added to methanol and stirred for 5 min before addition of TEOS, which was left to react for one hour at 20 °C. NPs with an average size of ~100 nm were synthesized by tailoring the reactant concentrations.⁷⁰ The NP suspensions were then washed three times by centrifugation using isopropanol, dried under vacuum and stored as powders in sealed glass vials. For each measurement, the NPs were dispersed at a concentration of 2 mg/mL using an ultrasonic probe (CPX 130, Cole-Parmer Instruments, IL) at 190 J and for 10 s twice, and further diluted to a final concentration of 0.5 mg/mL. NP suspensions were prepared in sterile-filtered 5-10 mM phosphate solutions adjusted to pH 4, 6.5, 8 and 10. NP size and ζ -potential were measured using a Zetasizer Nano (Malvern Instrument, UK). A CPS 20000 disc centrifuge, calibrated using 377 nm diameter PVC

particles (instrument and calibrant supplied by CPS Instruments Inc., LA), was used to conduct the differential centrifugal sedimentation (DCS) measurements. The density gradient within the disc was built according to manufacturer instructions. The density of the sucrose (Amresco LLC, OH) solution varied between 8 and 24 wt %. A volume of 100 μL and a concentration of $\sim 10^{10}$ particles/mL, in DI water, was used for each run and the disc was recalibrated every three runs. The particle size distribution was measured in triplicate within one gradient lifetime. Assumptions relating to the material properties of bulk silica used in the operating procedure included the Stöber silica density of 2.0 g/cm^3 , the refractive index of 1.45, and the absorption of 10^{-3} at $\lambda \sim 405 \text{ nm}$.

Peptide films: Silicon substrates with a thermally grown surface layer (thickness $\sim 10 \text{ nm}$) of silicon dioxide were UV/ozone cleaned prior to evaporation with $\sim 10 \text{ nm}$ of chromium and $\sim 50 \text{ nm}$ of gold. Freshly evaporated gold substrates were incubated overnight in a solution containing $10 \mu\text{M}$ peptide and $1 \mu\text{M}$ methylated polyethylene glycol (PEG) -thiol molecules (SH-PEG₄-CH₃), rinsed with ultrapure water and blow dried with argon. Following the same procedure, control surfaces were prepared using PEG molecules only. Peptide-functionalised surfaces were characterised by X-ray photoelectron spectroscopy (XPS, AXIS Ultra, Kratos Analytical, UK). Peptide-functionalised and control surfaces were incubated overnight in the NP suspensions, rinsed with diluted phosphate solutions or ultrapure water and blow dried with Ar gas. Such prepared substrates were analysed by SEM (SUPRA FESEM, Carl Zeiss Microscopy, Germany).

III. RESULTS AND DISCUSSION

A. AFM force mapping using peptide-functionalised probes

In AFM force mapping, FDCs are measured over an array of points on the surface under investigation.³¹ From the FDCs recorded at each point, maps of the surface height variations and of the adhesion force are extracted. The height results from the distance at which the set peak force is obtained, and the adhesion force results from the depth, F_{po} , of the pull-off peak (Fig. 1(b)) occurring upon retraction of the probe from the surface. The spatial resolution is limited as the acquisition times are much longer than with most AFM imaging modes and a comparatively low pixel resolution needs to be chosen. Otherwise, the acquisition time amounts to several hours and the measurement can be impaired by thermal or electrical drift effects.

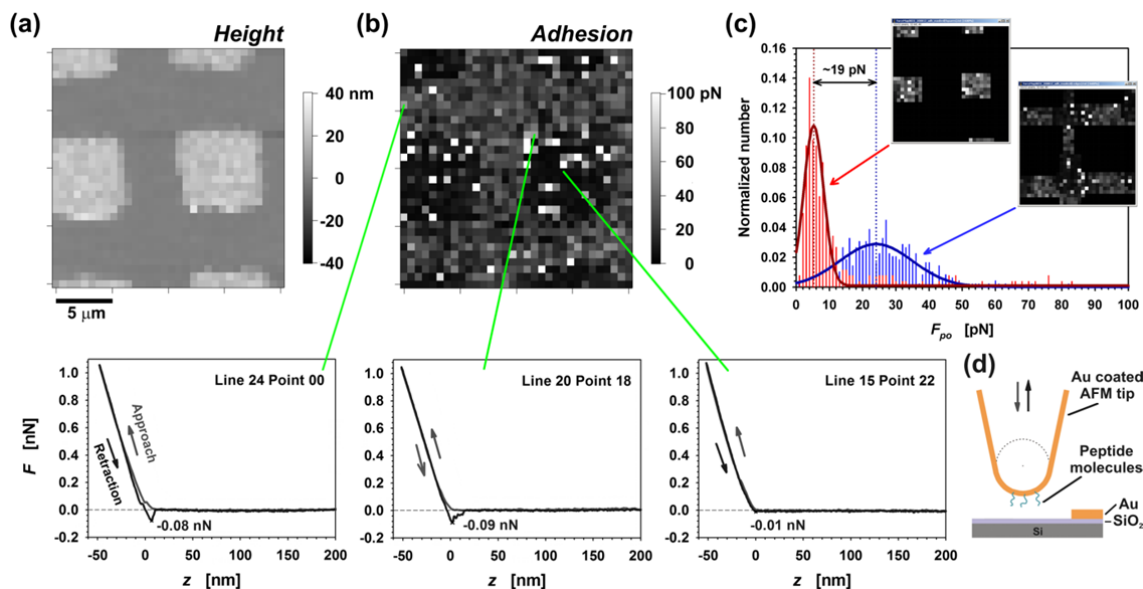


FIG. 1. Results of force mapping on the test sample, using an integrated AFM tip functionalised with the SiO₂ binding oligopeptides gSi4-1. (a) Height map (32x32 pixels), (b) adhesion map with three typical FDCs, and (c) histogram of the adhesion force distributions associated with the Au squares (plot in red) and surrounding SiO₂ surface (plot in blue), respectively. The curves resulted from Gaussian fits to both distributions. The adhesion map

is given by the pull-off peak magnitude, F_{po} , of FDCs measured at the pixel positions. (d) Schematic of a functionalised AFM tip over the patterned surface of the test sample.

Maps of the surface height variations and the adhesion force measured with an AFM tip (Fig. 1(d)) that had been functionalised with a silica-binding peptide are shown in Figs. 1(a) and 1(b), respectively. A square grid can be seen with a generally lower adhesion force in the square-shaped areas and a higher adhesion force in the areas between the squares. The corresponding height map in Fig. 1(a) shows that the squares are elevated by $\sim(19 \pm 5)$ nm, as expected for the gold coated areas on top of the wafer surface.

Digital masks corresponding to the Au squares and the areas in between (bare SiO₂ wafer surface) were selected for statistical analysis. The masked adhesion maps are shown as insets to Fig. 1(c), in which the greyscale has been renormalized. Areas that were not accounted for are in black. To eliminate contributions from step edges where the probe-sample contact area is ill-defined, the pixels next to the square edges were omitted. The histogram resulting from an adhesion force map shows two distributions as illustrated in Fig. 1 (c), and the gap between the peaks of both distributions is a measure for the adhesion contrast $\Delta F_{po} = F_{po}^{SiO_2} - F_{po}^{Au}$. In the case of Fig. 1(c) this is ~ 19 nN (for uncertainties see Table 2 and the discussion below). It should be noted that the distributions are slightly skewed as there are non-zero contributions to the right side of the peak which are not fully covered by the Gaussian fits. However, the resulting values of the most likely pull-off force of ~ 5 and ~ 24 pN (Table 2) are in good agreement with the median values of ~ 7 and ~ 25 pN, respectively. In contrast, the arithmetic mean is more susceptible to the presence of distribution tails and thus yields larger values of ~ 21 and ~ 27 pN, respectively.

It is conceivable that a background of non-specific binding makes a contribution to the total binding force measured. To suppress this effect, the buffer solution contained ~ 0.2 wt% of

the non-ionic surfactant Tween20.^{15, 67} Yet a non-zero offset due to remaining non-specific contribution to the measured F_{po} values may occur. A measure for this offset is the average F_{po} value of ~ 5 pN measured on the Au squares (Fig. 1(c) and Table 2). Assuming that this non-specific offset was similar for both the Au and SiO₂ surfaces, the adhesion contrast, ΔF_{po} , was due to the oligopeptide-surface interaction and is likely to scale with the number of oligopeptides capable of interacting with the surface. Thus, larger diameter probes will show higher adhesion forces and this is consistent with the findings we present later (see Fig. 4 and the related discussion).

To confirm that the observed adhesion force contrast can be attributed to the oligopeptide gSi4-1, the same measurements were carried out using probes functionalised with alternative sequences (Figs. 2, S2 and 3) as well as bare probes with no functionalisation other than the gold coating (Figs. S3 and S4). The alternative oligopeptides analysed were the stochastic sequence gSi4-1s with the same sum formula as gSi4-1 but a random sequence of amino acid residues (scrambled sequence) and the all-histidine sequence gHis12. In all these control experiments, no significant contrast was observed.

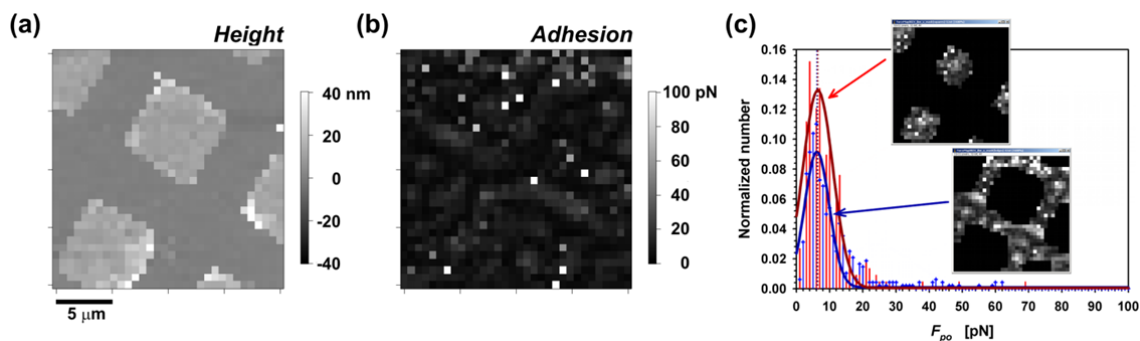


FIG. 2. Results of force mapping on the test sample, using an integrated AFM tip functionalised with the scrambled oligopeptides gSi4-1s. (a) Height map, (b) adhesion map, and (c) histogram of the adhesion force distributions associated with the Au squares (plot in red) and surrounding SiO₂ surface (plot in blue), respectively.

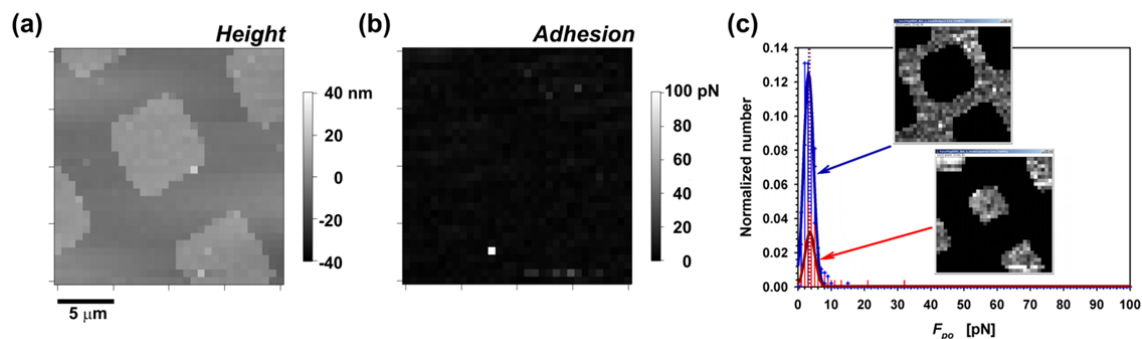


FIG. 3. Results of force mapping on the test sample, using an integrated AFM tip functionalised with the all-histidine oligopeptides gHis12. (a) Height map, (b) adhesion map, and (c) related histogram of the adhesion force distributions associated with the Au squares (plot in red) and surrounding SiO₂ surface (plot in blue), respectively.

Similarly to the adhesion force, the lateral force was found to be larger on silica surfaces than on Au surfaces (Fig. 4(b)). The lateral force is measured via the torsional deformation of the cantilever and results from the friction force acting in the tip-sample contact when dragging the tip across the surface. Such an LFM image is measured in contact mode which also yields a topography image (Fig. 4), reflecting the height adjustments required to maintain a constant deflection of the AFM cantilever.

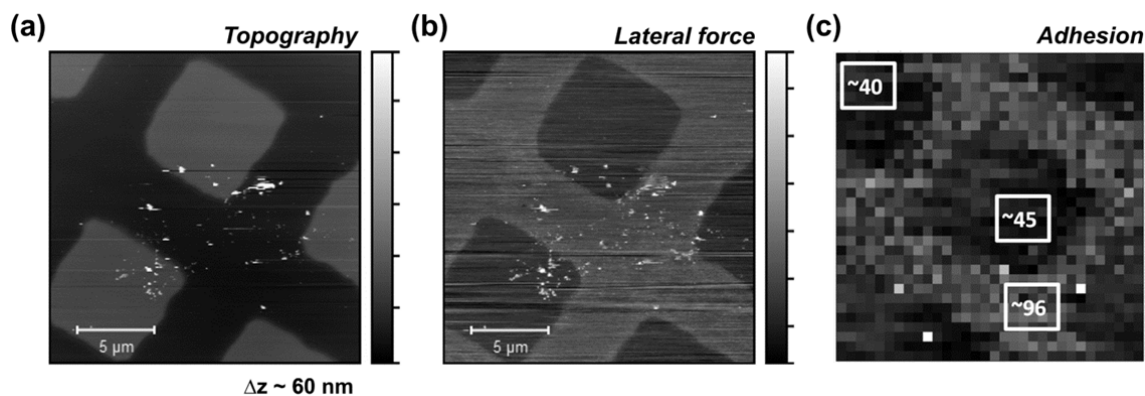


FIG. 4. Results of AFM measurements using an AFM tip functionalised with the silica-binding oligopeptides gSi4-1. (a) Topography image of an array of Au squares (height ~ 12 nm) on top of a silica surface. The scan width and pixel number are $20 \mu\text{m}$ and 256×256 ,

respectively. (b) Corresponding LFM image, accounting for the lateral force signal measured both upon trace and retrace through $(V_{lat}^{tr} - V_{lat}^{retr})/2$. (c) Adhesion map of another area of the same surface. The scan width and pixel number are 20 μm and 32x32, respectively. The numbers given are in units of pN and are the average F_{po} values of the marked areas.

For a microscopic contact with adhesive interactions between both surfaces, the friction force, F_f , can be described by the Bowden-Tabor model.^{71,72} It states that F_f scales with the contact area, A , and the interfacial shear strength, τ , as a constant factor, i.e. $F_f = \tau A$. As sliding motion of the AFM tip across the surface involves continuous formation and rupture of "bonds" across the tip-sample contact, τ is expected to increase with the adhesion forces and has been found to scale with the interfacial adhesion energy.^{72,73,74} In addition, through the scaling with the contact area, F_f also depends on the elastic-plastic deformation behaviour of the contact and the roughness of the mating surfaces. Consistently, in the case of an AFM tip functionalised with the scrambled peptide gSi4-1s which shows negligible adhesion contrasts, no friction contrast has been observed between the gold and silica areas (Fig. S5 in the *Supplementary Material*). Considering the correspondence between the adhesion (Figs. 1(b) and 4(c)) and the friction (Fig. 4(b)) contrasts observed, i.e. a higher friction force is measured where the adhesion force is increased, it may be concluded that the differences in deformation or roughness between Au and silica surfaces played a minor role, if any (see Sec. S.1 in the *Supplementary Material* for further discussion).

The results from the CFM measurements are summarised in Table 2 which gives the centre values and the widths of the Gaussian fits to the distributions. The ratio of the adhesion contrast between the Au and SiO₂ areas, ΔF_{po} , and the mean peak width of the adhesion force histograms, w , is also included. A value greater than ~ 1 indicates that the observed contrast is significant. Clearly, a difference is found between the adhesion behaviour of the initial sequence gSi4-1 ($|\Delta F_{po}/w| > 1$) and all other functionalisation types investigated ($|\Delta F_{po}/w|$

< 0.5). In particular, in the case of gSi4-1s no significant adhesion contrast was observed (Figs. 2 and S2). This is noteworthy since gSi4-1s is a randomised version of gSi4-1, i.e. it differs from gSi4-1 only in the order of amino acids. Thus, this finding suggests that the particular sequence of amino acids is critically important for the distinct adhesion behaviour displayed by gSi4-1 (Figs. 1, 4 and S1).

TABLE 2. Overview of the adhesion mapping results.

Probe functionalisation	Probe type	F_{po}^{Au} ^a [pN]	ΔF_{po} ^b [pN]	w ^c [pN]	$\Delta F_{po} / w$ [pN]
SiO ₂ binding gSi4-1	Tip	5	19	8	+2.4
	Colloidal	28	163	145	+1.1
Scrambled gSi4-1s	Tip	6	-0.2	5	0.0
	Colloidal	18	-2.2	5	-0.4
All-histidine gHis12	Tip	4	-0.4	2	-0.2
Bare	Tip	6	0.4	3	+0.1
	Colloidal	23	-0.3	7	-0.0

^a Centre value of Gaussian fit to distribution associated with Au surface

^b $\Delta F_{po} = F_{po}^{SiO_2} - F_{po}^{Au}$

^c w - Arithmetic mean of FWHM/2 values of both the Gaussians associated with the SiO₂ and Au surfaces

It should be borne in mind that the measured adhesion force scales with the number of peptide molecules interacting with the sample surface. That is, in a linear approach the total adhesion force can be written as a multiple of the average adhesion force per peptide molecule (plus a non-zero offset if non-specific binding occurs). In the case of the adhesion map shown in Fig. 4(c), the average adhesion force was ~43 pN on Au coated areas and

~ 96 pN on silica areas. Thus, on SiO_2 the average adhesion force was increased by $\Delta F_{po} \sim 53$ pN, i.e. the adhesion force difference was ~ 3 times larger than in the case of Fig. 1(b).

Furthermore, in the case of a measurement using a colloidal probe functionalised with the silica-binding oligopeptide (Fig. S1(c) in the *Supplementary Material*), the adhesion force difference was $\Delta F_{po} \sim 160$ pN and thus ~ 8 times larger than in the case of Fig. 1(b). Indeed, the larger radius ($R \sim 1.5 - 3 \mu\text{m}$) of the colloidal probe should present a bigger number of oligopeptide molecules to the sample surface and thus allow a larger adhesion force. Small variations in the area density of oligopeptides on the surface of the AFM tip or colloidal probe may cause a departure from exact scaling of the measured adhesion force with the probe radius, R . For instance, such variations may result from the non-zero surface roughness of a colloidal probe.

Finally, it is interesting to compare the measured adhesion difference of $\Delta F_{po} \sim 19$ pN (or multiples thereof) between Au and SiO_2 areas (Fig. 1(c)) to typical values of bond rupture forces, bearing in mind that measured bond rupture forces are a function of the unloading rate.²⁷ Approximately, they are ~ 2000 pN for the covalent bond between silicon and carbon⁷⁵, ~ 100 to 200 pN for a biotin-streptavidin pair (see⁷⁶ and references therein) as an example for a ligand-receptor pair, and in the range of ~ 1 to 8 pN for a single hydrogen bond⁷⁷. Hence, one may surmise that the observed adhesion force difference of ~ 19 pN (Fig. 1(c)) is equivalent to several hydrogen bonds. However, assigning the adhesion force difference to a single type of interaction could be misleading, as several force contributions may occur alongside each other, such as hydrogen bonds and electrostatic interactions. Notably, the total interaction force measured seems to include non-zero contributions from non-specific interactions (Table 2), such as van der Waals forces or hydrophobic attraction occurring in aqueous solution. The possibility of combined interactions has also been emphasized by Hara and co-workers.^{15, 16} For the specific interaction between their titanium binding peptide and a

Ti/TiO₂ surface, measured in water, they reported a combination of two electrostatic interactions and one hydrogen bond.

B. Adsorption of nanoparticles on peptide thin films

Gold surfaces functionalised with gSi4-1 were analysed by XPS. Representative survey and high resolution spectra are shown in Fig. S6 in the *Supplementary Material*. XPS data were analysed⁷⁸ and an average thickness of ~2.2 nm was obtained for the peptide layer, as described in Sec. S.2 in the *Supplementary Material*. This result is consistent with the hypothesis of a single peptide layer adsorbed onto the gold surface. Peptide monolayers were exposed to an aqueous suspension containing 100 nm silica NPs dispersed in a buffer similar to that used for the CFM experiments. Figure 5(a) shows a typical SEM image of such surfaces after they were rinsed to remove any loosely bound particles.

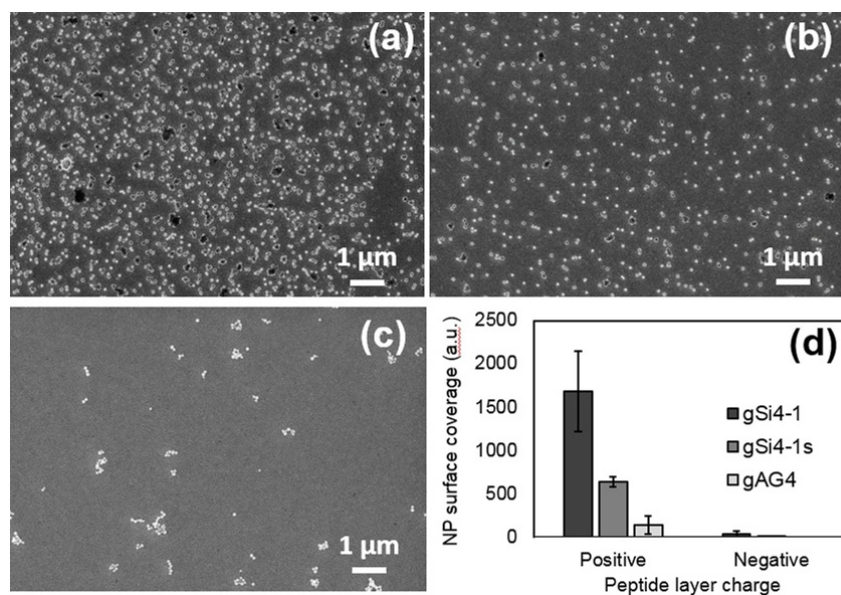


FIG. 5. Representative SEM images of (a) gSi4-1 and (b) gSi4-1s and (c) gAG4 layers after overnight incubation in suspensions containing 100 nm SiO₂ NPs at acidic pH. (d) Relative surface coverage of the SiO₂ NPs on the peptide layers after incubation at pH conferring a positive (pH 4) and negative (pH 10) charge to the peptide layers.

The surface appears to be covered with NPs. XPS analysis of the samples confirmed that the particles were made of silica (results not shown). Furthermore, image analysis confirmed that the size of the NPs was consistent with results from differential centrifugal sedimentation (DCS) analysis performed on the NPs in solution (see Fig. S7 in the *Supplementary Material*). It can be inferred that the SiO₂ NPs adsorbed on the gSi4-1 peptide layer. When the same experiment was performed using a peptide layer made of gSi4-1s peptides, we also observed adsorption of NPs, but to a lesser extent. This is consistent with CFM results, where the affinity of gSi4-1s functionalised cantilever probes for silica was reduced with respect to the gSi4-1 peptide. However, the adsorption of silica NPs is significant on gSi4-1s peptide surfaces, at almost 40% of that measured on gSi4-1 surfaces. It seems likely that electrostatic interactions and hydrogen bonding through the H residues play a major role in the interaction of the NPs with the peptide layers. The number of positively charged residues in peptides has been found to influence their ability to attract silica NPs.⁷⁹ For example, several engineered peptides showing a high affinity to thermally grown silica have been presented by Eteshola et al.⁴⁶ They noted enhanced levels of H in most of their peptides whereas the frequency of other basic amino acids, such as K and R⁴⁵, did not change significantly with selection. Because both gSi4-1 and gSi14s peptides have 5 H residues each, it is possible that the interaction between the silica NPs and the peptide monolayers is influenced by the overall content of H residues. When a peptide free of H residues was used to form the peptide layers, namely the peptide gAG4 which is known for binding silver⁶⁴, SiO₂ NP adsorption was ~8.5% of the NP density observed on gSi4-1 peptide layers. A representative SEM image is shown in Fig. 5(c).

The measurements described so far were performed at a pH below the isoelectric point of the peptides, which is pH 8 for the gSi4-1 and gSi4-1s peptides and pH 6.5 for the gAG4 peptides (see Table 1). At acidic pH, protonation of the peptides is expected to confer a

positive charge to the peptide layers. On the other hand, the silica NPs have a negative charge over a wide range of pH^{47, 79, 80, 81} due to partial ionization of the surface silanol groups by trapping of OH⁻ ions^{81, 56, 82, 83}, thus resulting in the formation of Si=(OH)₂⁻ species that allow anionic hydrogen bonding^{56, 82}. We measured a ζ -potential of the SiO₂ NPs varying from \sim -22 mV at pH 4 to \sim -56 mV at pH 11. Possibly, unspecific attractive electrostatic forces contribute to the adsorption of the SiO₂ NPs onto the peptide surfaces. It should be noted that at acidic pH NPs may be more prone to agglomeration, as a maximum in adhesion between silica surfaces has been observed⁸², which is consistent with the more positive ζ -potential values we measured at this pH. To test this hypothesis, the adsorption of the NPs onto the peptide layers was attempted while dispersing the NPs in a solution having alkaline pH (pH 10). At this pH, the peptide layers are expected to bear an overall negative charge, while the SiO₂ NPs are also negatively charged. As shown in Fig. 5(d), a very low adsorption of NPs was observed on these surfaces, which would suggest that, in this pH regime, the electrostatic repulsion dominates the interaction between the peptides and the NPs. The level of NP adsorption observed at alkaline pH was comparable to that observed on surfaces covered with only methylated PEG (results not shown) and close to zero.

We conclude that in the case of adsorption of NPs on peptide layers the electrostatic effects are important, but there is clear evidence here for an additional specific interaction between the gSi4-1 peptide and the silica particles. This is consistent with the CFM results, which were also performed under slightly acidic conditions conferring a net positive charge to the peptides. Compared to the case of extended peptide films on a flat substrate, however, in the case of CFM using AFM tips the peptides are attached to the highly curved surface of a nano-scale tip. In this geometry, the peptides are likely to be less crowded than in the case of a peptide monolayer on a flat surface, which would suggest that the segmental mobility is increased and thus a binding amino acid sequence more readily exposed to the silica surface.

Furthermore, the presence of surfactant Tween20 in the CFM experiments should have weakened the electrostatic interaction^{15,67}, which may explain the reduced force of interaction observed for the scrambled peptide sequences gSi4-1s compared to the case of extended surfaces.

C. *Monitoring the adsorption of nanoparticles on peptide-functionalised microcantilevers*

Here, we test whether the adsorption of SiO₂ NPs onto a surface can be monitored through the measurement of changes in resonance frequency of a microcantilever immersed into a suspension containing the NPs. This approach has the advantage of potentially being in-line integrable into a device to provide both a simultaneous and quantitative response to the presence of specific NPs suspended in a liquid medium.

The surface of the micro-cantilever was functionalised with the SiO₂-binding peptide, similarly to the force mapping experiments described in Sec. III.A. Upon adsorption of NPs, the total mass of the AFM cantilever will increase and thus its fundamental resonance frequency decrease. Adsorption induced mass changes can thus be monitored via changes in the resonance frequency of the oscillator, similar to a quartz crystal microbalance.^{84,85}

To allow a larger sensitivity, ultra-small cantilevers with a length of ~38 μm were used.

Owing to their small size and mass, an increase in their total mass, Δm , caused by NP adsorption results in a relatively large change in resonance frequency, Δf . Neglecting hydrodynamic considerations, the mass sensitivity, $\Delta f / \Delta m$, of a rectangular cantilever scales with $1/(WL^3)$, where W and L are the width and the length of the cantilever, respectively.^{86,}

⁸⁷

After functionalisation of the cantilever with the SiO₂ binding peptide, its thermomechanical spectrum was measured in plain buffer to establish a value for the initial resonance frequency

under equivalent conditions. Then the cantilever was immersed into the SiO₂ NP suspension with a concentration of NPs of ~1.0 or 0.5 mg/mL. For each experiment a new cantilever was used. In the case of the measurements shown in Fig. 6, the average peak frequencies measured in the plain buffer were ~21.82 kHz and 21.79 kHz, respectively. No significant variation was observed over a period of ~40 min. After immersion of the cantilever into the NP suspension, however, strong variations in its peak frequency were observed which can be described in terms of an initial drop and a subsequent linear decrease at a constant rate over the period covered. The first measurement was taken ~4 min after immersion of the cantilever, since the time resolution of the series was limited by the acquisition time for thermomechanical noise spectra which were accumulated to obtain a sufficient signal-to-noise ratio. The initial drop, Δf_i , was ~0.11 and ~0.71 kHz for the concentrations of 0.5 and 1.0 mg/mL, respectively.

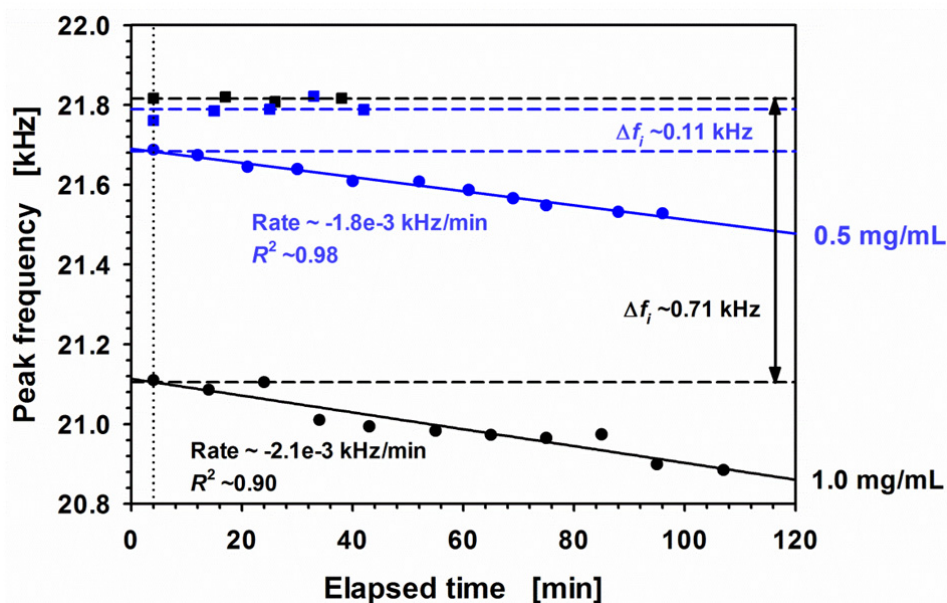


FIG. 6. Changes in the resonance frequency of a cantilever (type BL-AC40TS) functionalised with the SiO₂ binding peptide (type gSi4-1), as a function of the elapsed time. The response was measured for concentrations of 0.5 (blue circles) and 1.0 mg/mL (black circles) of the NP suspension containing SiO₂ NPs. Linear fits (solid lines) yield rates for the resonance frequency variations (R^2 - coefficient of determination). Data from reference measurements

taken in the plain buffer solution, i.e. without NPs added, are shown as blue and black squares, respectively. An initial frequency drop, Δf_i , is observed which is larger in the case of 1.0 mg/mL. The pH of both the plain buffer and the NP suspension was ~ 5.5 .

For both concentrations, the peak frequency was found to decrease over the monitored period of time (≤ 120 min) in a linear manner, with a rate of ~ -2 Hz/min (Fig. 6). This finding implies that the adsorption of NPs on the cantilever surface occurred at a constant non-zero rate. In contrast, control experiments (Fig. S8 in the *Supplementary Material*) using non-functionalised cantilevers of the same type showed relatively flat curves, e.g. in the case of 0.5 mg/mL concentration the decrease in peak frequency over time was negligible (in the order of 10^{-2} Hz/min). Furthermore, a non-zero but comparatively small initial frequency drop, Δf_i , of ~ -0.07 kHz was observed in both cases. In general, the observed frequency variations suggest adsorption kinetics with an initial non-linear regime of NP adsorption at high rates and a subsequent regime with adsorption at a lower but constant rate due to kinetic limitations on diffusion. Interpretation of the response of cantilevers of this type is not straightforward. As outlined in a theoretical study employing a mesoscopic model⁸⁸, the response of a cantilever sensor functionalised with an organic monolayer depends on several interactions, including elastic effects related to the different deformation behaviour of passive cantilever coatings, e.g. metal coatings, and the functional monolayer, as well as effects related to the surface charge density or conformational changes of the molecules and adsorbates.

IV. CONCLUSIONS AND OUTLOOK

In this study, the use of a SiO₂-binding engineered peptide has been explored for CFM on a patterned silica surface and selective NP capture:

- AFM force mapping using probes functionalised with SiO₂ binding peptides has shown an increased adhesion force on SiO₂ areas of a patterned test sample. Control experiments using a random permutation of the silica binding motif (scrambled sequence) and an all-histidine sequence confirmed the selective binding behaviour. The significantly smaller adhesion force measured in the case of the scrambled sequence demonstrated that the sequence order of residues plays an important role in establishing the recognition between the peptide and the silica surface, further to the sequence composition.
- LFM imaging undertaken concurrently, using the same AFM probe, showed an increased friction force on the silica areas, thus indicating that the friction between AFM probe and sample was dominated by the adhesive interaction. Importantly, the probe functionalisation was robust to the shear forces upon scanning and allowed stable contact mode imaging over one or more scans.
- The capture of SiO₂ NPs on peptide films was demonstrated. Electrostatic forces between the peptide layers and the silica NPs were found to play an important role in the adsorption of the NPs on the substrates. However, maximum adsorption was observed on the silica binding peptide layer, showing that the specific peptide motif was mainly directing the silica NP-peptide assembly.
- Functionalised AFM cantilevers immersed into a NP suspension with SiO₂ NPs showed a decrease in the fundamental cantilever resonance frequency, thus potentially enabling monitoring of the adsorption process.

Possible application areas where the selective capture of NPs via engineered peptides with specific binding affinity could be utilised are waste water treatment or the nano-scale assembly of hybrid materials. In addition, the selective binding behaviour of AFM probes functionalised with engineered peptides opens up new avenues for chemical mapping. With

such selective and reliable probe functionalisation techniques, AFM based chemical mapping in liquid can be a valuable addition to the available array of surface analytical techniques which are typically vacuum based. As demonstrated for the case of silica binding and mapping, engineered peptides bestow the required selectivity. Due to the large variety of known peptides with different documented binding characteristics, engineered peptides provide a versatile platform for a wide range of specific AFM probe binding chemistries. Further exploration of this route may well take CFM to a new level where probe functionalisation is highly specific and can be tailor-made by drawing from combinatorial peptide libraries.

ACKNOWLEDGMENTS

We are grateful to A.W. Booker for preparation of the test samples and to D. Gohil for technical support with the SEM imaging. We thank the Technology Strategy Board / Innovate UK for co-funding through a Feasibility Study for Responsible Development of Nanoscale Technologies and the National Measurement System of the UK Department for Business, Innovation and Skills for co-funding through the Innovation Research and Development Programme.

References

- ¹ C. Tamerler and M. Sarikaya, *ACS Nano* **3**, 1606 (2009).
- ² M.J. Olszta, X. Cheng, and S.S. Jee, **58**, 77 (2007).
- ³ A.B. Sanghvi, K.P.-H. Miller, A.M. Belcher, and C.E. Schmidt, *Nat. Mater.* **4**, 496 (2005).
- ⁴ S. Whaley, D. English, E. Hu, P. Barbara, and A. Belcher, *Nature* **405**, 665 (2000).
- ⁵ M. Sarikaya, C. Tamerler, A.K.-Y. Jen, K. Schulten, and F. Baneyx, *Nat. Mater.* **2**, 577 (2003).
- ⁶ S. Zhang, *Nat. Biotechnol.* **21**, 1171 (2003).
- ⁷ W.-S. Choe, M.S.R. Sastry, C.K. Thai, H. Dai, D.T. Schwartz, and F. Baneyx, *Langmuir* **23**, 11347 (2007).
- ⁸ F. Baneyx and D.T. Schwartz, *Curr. Opin. Biotechnol.* **18**, 312 (2007).

- ⁹ B. Zhou, Y. Liu, W. Wei, and J. Mao, *Med. Hypotheses* **71**, 591 (2008).
- ¹⁰ S. Brown, *Nat Biotech* **15**, 269 (1997).
- ¹¹ B.R. Peelle, E.M. Krauland, K.D. Wittrup, and A.M. Belcher, *Langmuir* **21**, 6929 (2005).
- ¹² H. Heinz, B.L. Farmer, R.B. Pandey, J.M. Slocik, S.S. Patnaik, R. Pachter, and R.R. Naik, *J. Am. Chem. Soc.* **131**, 9704 (2009).
- ¹³ R.L. Willett, K.W. Baldwin, K.W. West, and L.N. Pfeiffer, *Proc. Natl. Acad. Sci.* **102**, 7817 (2005).
- ¹⁴ U.O.S. Seker, B. Wilson, S. Dincer, I.W. Kim, E.E. Oren, J.S. Evans, C. Tamerler, and M. Sarikaya, *Langmuir* **23**, 7895 (2007).
- ¹⁵ T. Hayashi, K.-I. Sano, K. Shiba, Y. Kumashiro, K. Iwahori, I. Yamashita, and M. Hara, *Nano Lett.* **6**, 515 (2006).
- ¹⁶ Y. Arai, K.-I. Okabe, H. Sekiguchi, T. Hayashi, and M. Hara, *Langmuir* **27**, 2478 (2011).
- ¹⁷ C.E. Flynn, C. Mao, A. Hayhurst, J.L. Williams, G. Georgiou, B. Iverson, and A.M. Belcher, *J. Mater. Chem.* **13**, 2414 (2003).
- ¹⁸ C.K. Thai, H. Dai, M.S.R. Sastry, M. Sarikaya, D.T. Schwartz, and F. Baneyx, *Biotechnol. Bioeng.* **87**, 129 (2004).
- ¹⁹ Y. Shimada, M. Suzuki, M. Sugiyama, I. Kumagai, and M. Umetsu, *Nanotechnology* **22**, 275302 (2011).
- ²⁰ M.D. Roy, S.K. Stanley, E.J. Amis, and M.L. Becker, *Adv. Mater.* **20**, 1830 (2008).
- ²¹ A. Wierzbicki, C.S. Sikes, J.D. Madura, and B. Drake, *Calcif. Tissue Int.* **54**, 133 (1994).
- ²² E.M. Krauland, B.R. Peelle, K.D. Wittrup, and A.M. Belcher, *Biotechnol. Bioeng.* **97**, 1009 (2007).
- ²³ Z. Su, T. Leung, and J.F. Honek, *J. Phys. Chem. B* **110**, 23623 (2006).
- ²⁴ D. Khatayevich, C.R. So, Y. Hayamizu, C. Gresswell, and M. Sarikaya, *Langmuir* **28**, 8589 (2012).
- ²⁵ Y. Cui, S.N. Kim, S.E. Jones, L.L. Wissler, R.R. Naik, and M.C. McAlpine, *Nano Lett.* **10**, 4559 (2010).
- ²⁶ J.W. Jaworski, D. Raorane, J.H. Huh, A. Majumdar, and S.-W. Lee, *Langmuir* **24**, 4938 (2008).
- ²⁷ H.-J. Butt, B. Cappella, and M. Kappl, *Surf. Sci. Rep.* **59**, 1 (2005).
- ²⁸ A. Yacoot and L. Koenders, *J. Phys. D. Appl. Phys.* **41**, 103001 (2008).
- ²⁹ E.W. van der Vegte and G. Hadziioannou, *Langmuir* **13**, 4357 (1997).
- ³⁰ T.J. Colburn and G.J. Leggett, *Langmuir* **23**, 4959 (2007).
- ³¹ H.-J. Butt, B. Cappella, and M. Kappl, *Surf. Sci. Rep.* **59**, 1 (2005).
- ³² C.D. Frisbie, L.F. Rozsnyai, A. Noy, M.S. Wrighton, and C.M. Lieber, *Science* **265**, 2071 (1994).
- ³³ H. Hillborg, N. Tomczak, A. Oláh, H. Schönherr, and G.J. Vancso, *Langmuir* **20**, 785 (2004).
- ³⁴ A. Noy, *Surf. Interface Anal.* **38**, 1429 (2006).
- ³⁵ G. Meyer and N.M. Amer, *Appl. Phys. Lett.* **57**, 2089 (1990).

- ³⁶ M. Munz, E. Schulz, and H. Sturm, *Surf. Interface Anal.* **33**, 100 (2002).
- ³⁷ M. Munz, *J. Phys. D. Appl. Phys.* **43**, 063001 (2010).
- ³⁸ D.J. Müller and Y.F. Dufrêne, *Nat. Nanotechnol.* **3**, 261 (2008).
- ³⁹ N. Suzuki, L. Gamble, C. Tamerler, M. Sarikaya, D.G. Castner, and F.S. Ohuchi, *Surf. Interface Anal.* **39**, 419 (2007).
- ⁴⁰ S. Donatan, M. Sarikaya, C. Tamerler, and M. Urgan, *J. R. Soc. Interface* **9**, 2688 (2012).
- ⁴¹ J.S. Evans, R. Samudrala, T.R. Walsh, E.E. Oren, and C. Tamerler, *MRS Bull.* **33**, 514 (2008).
- ⁴² J. Feng, R.B. Pandey, R.J. Berry, B.L. Farmer, R.R. Naik, and H. Heinz, *Soft Matter* **7**, 2113 (2011).
- ⁴³ C.R. So, J.L. Kulp, E.E. Oren, H. Zareie, C. Tamerler, J.S. Evans, and M. Sarikaya, *ACS Nano* **3**, 1525 (2009).
- ⁴⁴ U.O.S. Seker, B. Wilson, J.L. Kulp, J.S. Evans, C. Tamerler, and M. Sarikaya, *Biomacromolecules* **15**, 2369 (2014).
- ⁴⁵ C - Cysteine, D - Aspartic acid, E - Glutamic acid, G - Glycine, H - Histidine, K - Lysine, M - Methionine, P - Proline, R - Arginine, S - Serine, T - Threonine, W - Tryptophan.
- ⁴⁶ E. Eteshola, L.J. Brillson, and S.C. Lee, *Biomol. Eng.* **22**, 201 (2005).
- ⁴⁷ T. Hayashi, K.-I. Sano, K. Shiba, K. Iwahori, I. Yamashita, and M. Hara, *Langmuir* **25**, 10901 (2009).
- ⁴⁸ F. Taraballi, A. Natalello, M. Campione, O. Villa, S.M. Doglia, A. Paleari, and F. Gelain, *Front. Neuroeng.* **3**, (2010).
- ⁴⁹ K. Goede, P. Busch, and M. Grundmann, *Nano Lett.* **4**, 2115 (2004).
- ⁵⁰ M. Murariu, E.S. Dragan, and G. Drochioiu, *Biopolymers* **93**, 497 (2010).
- ⁵¹ J.E. Coleman, *Annu. Rev. Biochem.* **61**, 897 (1992).
- ⁵² R.R. Naik, L.L. Brott, S.J. Clarson, and M.O. Stone, *J. Nanosci. Nanotechnol.* **2**, 95 (2002).
- ⁵³ B. Korzeniowska, R. Nooney, D. Wencel, and C. McDonagh, *Nanotechnology* **24**, 442002 (2013).
- ⁵⁴ J. Godoy-Navajas, M.P.A. Caballos, and A. Gómez-Hens, *Anal. Chim. Acta* **701**, 194 (2011).
- ⁵⁵ I.I. Slowing, B.G. Trewyn, S. Giri, and V.S.-Y. Lin, *Adv. Funct. Mater.* **17**, 1225 (2007).
- ⁵⁶ R.K. Iler, *The Chemistry of Silica* (Wiley-Interscience, New York, 1979).
- ⁵⁷ P. Manoudis, S. Papadopoulou, I. Karapanagiotis, A. Tsakalof, I. Zuburtikudis, and C. Panayiotou, *J. Phys. Conf. Ser.* **61**, 1361 (2007).
- ⁵⁸ R. Karmouch and G.G. Ross, *Appl. Surf. Sci.* **257**, 665 (2010).
- ⁵⁹ A. Braun, V. Kestens, K. Franks, G. Roebben, A. Lamberty, and T.P.J. Linsinger, *J. Nanoparticle Res.* **14**, 1021 (2012).
- ⁶⁰ J. Tuoriniemi, A.-C.J.H. Johnsson, J.P. Holmberg, S. Gustafsson, J.A. Gallego-Urrea, E. Olsson, J.B.C. Pettersson, and M. Hassellöv, *Sci. Technol. Adv. Mater.* **15**, 35009 (2014).
- ⁶¹ V. Kestens, G. Roebben, J. Herrmann, Å. Jämting, V. Coleman, C. Minelli, C. Clifford, P.-J. De Temmerman, J. Mast, L. Junjie, F. Babick, H. Cölfen, and H. Emons, *J. Nanoparticle Res.* **18**, 171 (2016).

- ⁶² B.J.H. Kuipers and H. Gruppen, *J. Agric. Food Chem.* **55**, 5445 (2007).
- ⁶³ Routine available online under http://www.genscript.com/ssl-bin/site2/peptide_calculation.cgi.
- ⁶⁴ R.R. Naik, S.J. Stringer, G. Agarwal, S.E. Jones, and M.O. Stone, *Nat. Mater.* **1**, 169 (2002).
- ⁶⁵ H.-J. Butt and M. Jaschke, *Nanotechnology* **6**, 1 (1995).
- ⁶⁶ R. Proksch, T.E. Schäffer, J.P. Cleveland, R.C. Callahan, and M.B. Viani, *Nanotechnology* **15**, 1344 (2004).
- ⁶⁷ K.L. Brogan, J.H. Shin, and M.H. Schoenfish, *Langmuir* **20**, 9729 (2004).
- ⁶⁸ E.B. W. Stober, A. Fink, *J. Colloid Interface Sci.* **26**, 62 (1968).
- ⁶⁹ J.W. Kim, L.U. Kim, and C.K. Kim, *Biomacromolecules* **8**, 215 (2007).
- ⁷⁰ N.C. Bell, C. Minelli, J. Tompkins, M.M. Stevens, and A.G. Shard, *Langmuir* **28**, 10860 (2012).
- ⁷¹ F. Bowden and D. Tabor, *The Friction and Adhesion of Solids - Part 2* (Clarendon Press, Oxford, 1964).
- ⁷² R.W. Carpick, N. Agraït, D.F. Ogletree, and M. Salmeron, *Langmuir* **12**, 3334 (1996).
- ⁷³ A good correspondence between adhesion and friction forces is also reported in Ref. [29], however, the friction force is not analysed in terms of the interfacial shear strength.
- ⁷⁴ N. Nikogeorgos, C.A. Hunter, and G.J. Leggett, *Langmuir* **28**, 17709 (2012).
- ⁷⁵ M. Grandbois, M. Beyer, M. Rief, H. Clausen-Schaumann, and H.E. Gaub, *Sci.* **283**, 1727 (1999).
- ⁷⁶ J. Zlatanova, S.M. Lindsay, and S.H. Leuba, *Prog. Biophys. Mol. Biol.* **74**, 37 (2000).
- ⁷⁷ B.D. Sattin, A.E. Pelling, and M.C. Goh, *Nucleic Acids Res.* **32**, 4876 (2004).
- ⁷⁸ A.G. Shard, *J. Phys. Chem. C* **116**, 16806 (2012).
- ⁷⁹ S. V Patwardhan, F.S. Emami, R.J. Berry, S.E. Jones, R.R. Naik, O. Deschaume, H. Heinz, and C.C. Perry, *J. Am. Chem. Soc.* **134**, 6244 (2012).
- ⁸⁰ H. Chen, X. Su, K.-G. Neoh, and W.-S. Choe, *Anal. Chem.* **78**, 4872 (2006).
- ⁸¹ A. Hozumi, H. Sugimura, Y. Yokogawa, T. Kameyama, and O. Takai, *Colloids Surfaces A Physicochem. Eng. Asp.* **182**, 257 (2001).
- ⁸² J.D. Batteas, M.K. Weldon, and K. Raghavachari, in *Nanotribology - Crit. Assess. Res. Needs*, edited by S.M. Hsu and Z.C. Ying (Kluwer Academic Publishers, Norwell, 2003), pp. 387–398.
- ⁸³ J. Bowen, M. Manickam, S.D. Evans, K. Critchley, K. Kendall, and J.A. Preece, *Thin Solid Films* **516**, 2987 (2008).
- ⁸⁴ G. Sauerbrey, *Zeitschrift Fur Phys.* **155**, 206 (1959).
- ⁸⁵ M. Rodahl, F. Höök, A. Krozer, P. Brzezinski, and B. Kasemo, *Rev. Sci. Instrum.* **66**, 3924 (1995).
- ⁸⁶ J.W. Yi, W.Y. Shih, and W.-H. Shih, *J. Appl. Phys.* **91**, 1680 (2002).
- ⁸⁷ S. Li, L. Orona, Z. Li, and Z.-Y. Cheng, *Appl. Phys. Lett.* **88**, 073507 (2006).
- ⁸⁸ M.L. Sushko, *Faraday Discuss.* **143**, 63 (2009).